ChemComm

COMMUNICATION

View Article Online
View Journal | View Issue

Cite this: *Chem. Commun.*, 2020, **56**, 2779

Received 4th December 2019,
Accepted 28th January 2020

DOI: 10.1039/c9cc09426a

rsc.li/chemcomm

Carrier dynamic monitoring of a π-conjugated polymer: a surface-enhanced Raman scattering method†

Xin-Yuan Zhang,[abc] Shuo Yang,[b] Lili Yang,[a] Daxin Zhang,[bc] Yansen Sun,[bc] Zhenyu Pang,[bc] Jinghai Yang *[a] and Lei Chen*[a]

Here, the carrier dynamics of a π-conjugated polymer is monitored by voltage-dependent surface-enhanced Raman scattering (SERS). The conductive polymer poly(3,4-ethylenedioxythiophene):poly(styrenesulfonate) (PEDOT:PSS) is employed as a metal-free SERS substrate. Under different voltage conditions, the SERS performance of the semiconductors' rectification characteristic is discussed. Our results open an unprecedented regime for conducting polymer-based SERS.

As energy issues have become a global concern, many efforts have been dedicated to improve the performance of solar cells.[1–3] However, the exploration of the interfacial dynamic process of carriers in solar cells has created massive confusion.[4] Recently, inorganic semiconductor-based SERS has emerged as a means to investigate the charge transfer process in solar-cell-like systems and estimate electron transfer behaviour, which means that SERS may be an essential method to discuss the charge transfer process at the interface in solar cell devices.[5–8] Nevertheless, effective integration of spectral characteristics into devices also requires more discussion under bias voltage conditions. To monitor the SERS performance of the dynamic process of carriers, especially with a bias voltage, a SERS-active substrate is essential.

SERS is a traditional approach with ultrasensitive detection and also plays a significant role in the biochemical and environmental fields. For traditional plasmonic SERS substrates, the electromagnetic field enhancement mechanism can be considered a main contribution: plasma is generated upon excitation by far-field incident light, and then the light is concentrated at the nanometre scale, which enhances the electromagnetic field around the nanoparticles (NPs). Then, NPs serve as optical antennas and propagate the Raman scattering frequency to the far field to enhance the Raman scattering signal.[9] Simultaneously, as a secondary contribution, the chemical enhancement mechanism, the Raman scattering signal will be enhanced by the charge transfer process between the SERS-active substrate and the adsorbate.[10] In 2017, Mehmet Yilmaz and colleagues synthesized a three-dimensional (3D) organic semiconductor, α,ω-diperfluorohexylquaterthiophene (DFH-4T); the SERS enhancement factor (EF) of this 3D organic molecule film was up to 10^3, almost reaching the theoretical maximum of a metal-free substrate.[11,12] It was verified that the enhancement for the small molecule DFH-4T is due to non-equivalent signal enhancements of analyte-specific binding geometry on the DFH-4T surface, as well as a charge-transfer transition between the probe molecule and the organic semiconductor substrate. This result confirmed the SERS activity of organic semiconductors and further perfected the basic SERS enhancement theory. Similarly, for a discussion of carrier performance in devices, here, we employ the π-conjugated conducting polymer PEDOT:PSS, which is widely used as a hole-transporting layer in photoelectric devices, as the SERS substrate.[13,14] Compared to DFH-4T, PEDOT:PSS possesses longer chains, as well as more ordered π–π stacking, which will facilitate and promote charge propagation along the main chain.[15] At the same time, its excellent electrical properties can be attributed to the π orbital electron delocalization of the conjugated structure.[16,17] As usual, under static conditions, the most commonly used microscopic model for the description of the carrier dynamics properties of conjugated polymers is based on the SSH tight-binding model, established by Su, Schrieffer and Heeger.[18–21] By contrast, under dynamic conditions, the establishment of a clear physical model has plagued many researchers for a long time, which has also caused much confusion during the charge transfer process.

On the basis of the above-mentioned premise, PEDOT:PSS was employed as the SERS-active substrate. To conduct an in-depth investigation into the chemical enhancement mechanism and evaluate the charge transfer process, methylene blue (MB)

[a] *Key Laboratory of Functional Materials Physics and Chemistry of the Ministry of Education, Jilin Normal University, Changchun 130103, P. R. China. E-mail: jhyang1@jlnu.edu.cn, chenlei@jlnu.edu.cn*
[b] *Changchun Institute of Optics, Fine Mechanics and Physics, Chinese Academy of Sciences, Changchun 130033, P. R. China*
[c] *University of Chinese Academy of Sciences, Beijing 100049, P. R. China*

† Electronic supplementary information (ESI) available: Experimental section, detailed enhancement factor calculation, AFM image of FTO/PEDOT:PSS/MB and optical photo of FTO/PEDOT:PSS/MB/Ag, SERS spectra of PEDOT:PSS/MB on FTO under the reverse bias-voltage conditions, the possible CT process, and tables showing assignments for the SERS spectra of MB on a substrate. See DOI: 10.1039/c9cc09426a

was selected as a probe molecule.[11,12] Surprisingly, the enhancement factor (EF) of the PEDOT:PSS film with a root-mean-square (RMS) of 1.81 nm can be up to 2.26×10^3. RMS is an important parameter of surface roughness. Such a value means that the smooth film will also exhibit excellent SERS activity. Then, SERS of PEDOT:PSS/MB is performed at various forward and reverse bias voltages to analyse the spectroscopic performance and rectification-like characteristics at semiconductor heterojunctions, as well as the different conductive PEDOT:PSS film under different voltage conditions. In addition, the intricate charge transfer processes under different voltage conditions were comprehended in a straightforward way. This work provides an important theoretical basis for the establishment of chemical enhancement models in SERS and a new idea for the exploration of photoelectric devices.

Here, a conducting polymer was used as a SERS-active substrate, which is not as common as precious metals and inorganic semiconductors. As a result, the fundamental enhancement capability and mechanism should be well studied. The scheme is illustrated in Fig. 1(a). It is known that morphology and roughness are extremely significant for SERS substrates,[22] and these parameters of a PEDOT:PSS film were obtained by atomic force microscopy (AFM), as shown in Fig. 1(b). The scanning area was $2 \times 2\ \mu m^2$, and the RMS was 1.81 nm, which indicates that the surface of the PEDOT:PSS film is extremely smooth. An AFM height image of MB molecules spin-coated on PEDOT:PSS with an RMS of 6.8 nm is shown in Fig. S1 (ESI†). This indicates that the surface roughness increases after the MB molecules are spin-coated; however, the contribution to SERS detection is still extremely low with such a roughness. The optical properties of PEDOT:PSS, MB and the mixture of PEDOT:PSS-MB were characterized by UV-vis absorbance spectroscopy, and the results are illustrated in Fig. S2 (ESI†). PEDOT:PSS retains the absorption on the red side at 500 nm, and the MB molecule has a strong absorption peak at ~655 nm.[23] Both of the above absorption characteristics are observed for the mixture; however, the maximum absorbance peak shifts to ~668 nm due to the coupling of the PEDOT:PSS and MB molecules.[7]

Raman spectroscopy and SERS of the substrates were conducted under 514 nm laser excitation, as shown in Fig. 1(c). The spectra of PEDOT:PSS and MB have been revealed in many previous studies, and all of the peak assignments are listed in Table S1 (ESI†).[24,25] The peaks assigned to PEDOT:PSS and MB were marked separately.

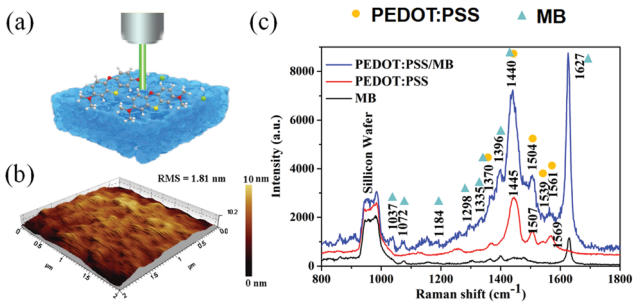

Fig. 1 (a) Schematic illustrations of the PEDOT:PSS/MB substrate. (b) AFM height image of PEDOT:PSS; the RMS is 1.81 nm. (c) Raman spectra of PEDOT:PSS, MB, and PEDOT:PSS/MB. The assignments for spectra are marked as yellow circles for PEDOT:PSS and blue triangles for MB.

As seen by comparing the SERS and Raman spectra of PEDOT:PSS, the peaks located at 1072, 1298, 1335, 1370, 1396, 1440, and 1627 cm^{-1} assigned to MB molecules are enhanced, especially the 1440 and 1627 cm^{-1} peaks. The peak at 1440 cm^{-1}, which is assigned to the asymmetric vibration of C–N, is enhanced and is attributed to both PEDOT:PSS and MB. This enhancement can be mainly considered a superposition of scattering peaks attributed to the PEDOT:PSS and MB molecules. The peak at 1627 cm^{-1} for MB is significantly selectively enhanced.[26] Additionally, the peak at 1627 cm^{-1} does not experience interference from the peaks of PEDOT:PSS, and it is truly the best choice for evaluating the enhancement factor. The calculated EF is 2.26×10^3 (a detailed calculation process is shown in the ESI†). Such an EF value is very excellent for this substrate. According to Mie theory, a smooth surface will greatly affect the scattering cross-section, which is detrimental to SERS enhancement.[5] Inherently, this can be explained by the properties of PEDOT:PSS.[27,28] The main reason for the high EF is π electron delocalization, which induced the chemical enhancement contribution upon laser excitation. The enhancement can be considered (i) a resonant enhancement coming from the formation of surface complexes or new chemical bonds by PEDOT:PSS and MB and (ii) a resonance-like enhancement of the photoinduced charge transfer from MB to PEDOT:PSS or from PEDOT:PSS to MB.[29,30] In addition, PEDOT:PSS is also regarded as a semimetallic material,[27] which means that upon laser excitation, a large number of excited-state electrons delocalize and oscillate collectively, which induces enhancement from the SPR contribution.[31] Thus, the combined effect of the two mechanisms (CT and SPR) allows the substrate to achieve a high EF for a limited cross-section.

As demonstrated above, PEDOT:PSS is an ideal candidate for a SERS-active substrate to further investigate the charge transfer process. For this reason, we evaluated the SERS performance of PEDOT:PSS/MB under various bias voltage conditions.[32] To bias the polymer and probe molecules, we treated PEDOT:PSS and MB with the same parameters on fluorine-doped SnO_2 (FTO) glass and then evaporated Ag on the surface as an electrode. Here, FTO serves as the cathode, and the Ag electrode is the anode. The AFM height image and an optical photograph of PEDOT:PSS/MB on FTO are shown in Fig. S3 (ESI†). After spin-coating the two layers, the substrate becomes blue, which is caused by the MB molecule, but is still transparent. The SERS spectra are illustrated in Fig. 2(a), and the scheme of the substrate with a bias voltage is shown in the inset of Fig. 2(a). Here, we set the reverse voltages from 0 to 5 V with a step of 0.5 V. Notably, the intensity of the peak at 1625 cm^{-1}, which can be assigned to the b_2 vibration mode of MB, is increased at a voltage of 0.5 V. As the voltage increases, the SERS intensity gradually decreases. Furthermore, the peaks at ~1401, ~1439, and ~1502 cm^{-1} are shifted. To further understand the enhancement mechanism, the numerical Raman shifts for different voltages at ~1439 cm^{-1} are listed as red points in Fig. 2(b) and described as reverse-biased. When we set the voltage to 0.5 and 1 V, the peak blueshifted and then redshifted with a further increase in voltage. As reported in our previous work, we found that the blueshift and redshift of the peak indicated an increase and decrease in the carrier density, respectively.[33]

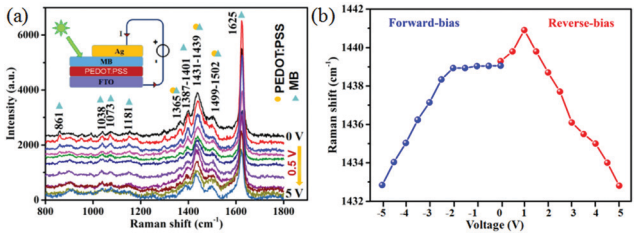

Fig. 2 (a) SERS spectra of PEDOT:PSS/MB on FTO under different bias voltage conditions. The yellow circles are the peaks contributed from PEDOT:PSS, and the blue triangles are the peaks assigned to MB. The inset shows the scheme. (b) The relationship between the voltage and Raman shift. The red part shows the peak positions for different voltage conditions at ~1439 cm^{-1} in (a); here, FTO is the cathode, and Ag is the anode. The blue part shows the SERS peak positions after swapping the positive and negative electrodes, where FTO is the anode and Ag is the cathode.

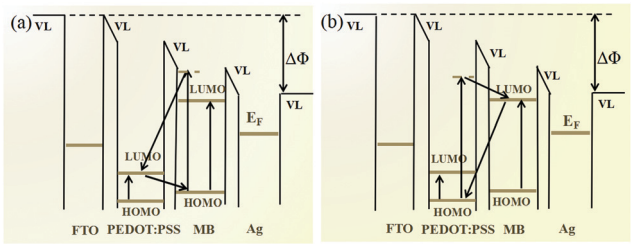

Fig. 3 The possible charge transfer processes between PEDOT:PSS and MB under reverse-bias conditions (the result illustrated in Fig. 2(a)). To balance the system, we tilt the vacuum level.

Here, when we reverse the voltage, the current flows from MB to PEDOT:PSS. In fact, PEDOT:PSS acts as an electron donor, and can also be considered a p-type semiconductor; additionally, MB molecules contain electron-withdrawing groups, which can be seen as n-type semiconductors. That is, a reverse voltage is applied across the heterojunction. Initially, the resistance of the built-in electric field is extremely large. From the perspective of carriers, the holes (cations) and electrons (anions) will be limited to the p-region and n-region, respectively.

The carriers are continuously accumulated by the resistance of the built-in electric field, which induces the peak blueshift. As the voltage continuously increases, the built-in electric field is not sufficient to resist the energy of the applied electric field yet, and the current will increase. At this time, a portion of the carriers will move directionally under the effect of a current impulse, and the number of carriers participating in the charge transfer process of SERS is reduced, leading to a change in polarizability, which redshifts the peak. Additionally, it is undoubted that as the carriers accumulate, an increasing SPR-induced hot electron transfer will contribute to the enhancement of the SERS signal under 514 nm laser illumination.[33,34] To further verify these theories, we swapped the positive and negative electrodes to make the current flow forward through the heterojunction (the obtained SERS spectra are shown in Fig. S4, ESI†). We also plot the relationship between the Raman shift and voltage in Fig. 2(b); the result is marked in blue and named forward bias. The result shows that the SERS intensities also increase when we apply a voltage of 0.5 V; however, the SERS signal does not shift initially, and linear-like changes are observed later when we increase the voltage. According to a previous analysis, voltage can provide a driving force for the orientated movement of positive and negative charges. When the voltage is small, the driving force is not large enough to affect the photogenerated carriers in the CT process of SERS, and the peak located at ~1439 cm^{-1} will remain stable. Then, with a continuous increase in the current, some of the photogenerated carriers in dynamic equilibrium will undergo drift motion, resulting in fewer carriers during CT and resulting in a significant redshift of the SERS peak. In addition, when the voltage is not large enough, the appearance of the blending layer and defects during preparation will also generate a built-in electric field, which hinders the redshift of the peak to some extent. In fact, this discussion was the basis for the spectroscopic performance of the rectification characteristics of an organic semiconductor heterojunction.

Then, the possible charge transfer processes between PEDOT:PSS and MB are analysed in detail. Under bias-voltage conditions, all the energy levels will tilt to reestablish equilibrium.[35] However, to simplify the analysis, we approximate the tilt of the vacuum level as shown in Fig. 3(a) and (b).[36–38] There are two possible routes for the charge transfer process. Under 514 nm laser illumination, the electrons of MB are excited to a higher state, then transfer to a matching lowest unoccupied molecular orbital (LUMO) level of PEDOT:PSS through resonance tunnelling, and finally transfer back to the highest occupied molecular orbital (HOMO) level of MB, releasing a Raman photon (Fig. 3(a)). In another case (Fig. 3(b)), the electrons of PEDOT:PSS are excited and then transferred to the LUMO of MB and then return to the HOMO of PEDOT:PSS, emitting a Raman photon[25,39] In addition, when we apply additional voltage, the Fermi level of the metal will be closer to the vacuum level, and $\Delta\phi = qU$.[37,40] When the forward-bias voltage is applied, the possible routes of CT are as shown in the ESI.†

Conductivity is a physical quantity that describes the difficulty of charge movement, and a higher conductivity will benefit the charge transfer process of SERS. Jianyong Ouyang's group reported that HCl treatment is an efficient method to change the conductivity of PEDOT:PSS.[41,42] After PEDOT:PSS was treated with HCl, the interaction between PEDOT and PSS was lower; moreover, the acid assisted in the removal of poorly conductive PSS.[42] Here, we treated PEDOT:PSS with 0, 0.25, 0.5, and 1 M HCl and then spin-coated MB, followed by evaporation of the Ag electrode; SERS spectra with a reversed 1 V bias voltage are shown in Fig. 4(a). After

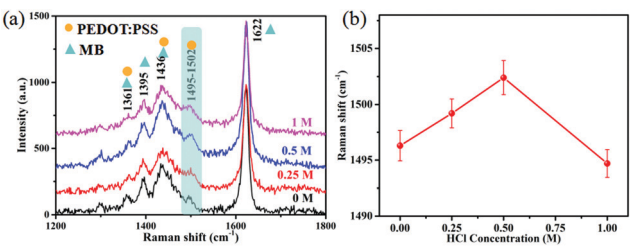

Fig. 4 (a) SERS spectra of FTO/PEDOT:PSS/MB/Ag, where PEDOT:PSS was treated with 0, 0.25, 0.5, and 1 M HCl; the yellow circles indicate the peaks contributed from PEDOT:PSS, and the blue triangles indicate the peaks assigned to MB. (b) The relationship between the HCl concentration and Raman shift at ~1497 cm^{-1}.

treatment with HCl, the SERS peak at $\sim$1497 cm^{-1} shifted. The relationship between the HCl concentration and the Raman shift is plotted in Fig. 4(b). As shown, the SERS peak was blueshifted and then redshifted significantly with increasing HCl concentrations. With an HCl concentration of 0.5 M, the value of the Raman shift is maximal. It can be considered that by biasing FTO/PEDOT:PSS(HCl)/MB/Ag, the cations and anions are limited to the p-region and n-region, respectively. A higher conductivity will result in more carrier accumulation and a greater blueshift. However, when the concentration of HCl continues to increase, the PEDOT:PSS layer and even FTO will be corroded, which will affect the electron transport process of the entire substrate.[42] Reducing the number of accumulated carriers correspondingly reduces the redshift of the SESR peaks. This result corresponded to the dynamic process of carriers under bias-voltage conditions by SERS.

In summary, we creatively employed the π-conjugated polymer PEDOT:PSS as a SERS substrate and discussed the spectroscopic performance of the carriers' dynamic process for different bias voltages and various conductivity conditions. In addition, two possible CT processes at different bias voltages were mentioned. This demonstration provides a new idea for the further exploration of SERS substrates, suggests SERS applications in the field of optoelectronic devices, and promotes the continuous development of Raman detection in devices.

This work was supported by the National Natural Science Foundation of China (No. 61775081, 61575080, and 61405072), the National Key Research and Development Program of China (Grant No. 2017YFF0108607), the Program for the Development of Science and Technology of Jilin province (Item No. 20180519016JH) and the Project of Jilin Development and Reform Commission (2019C051-3).

Conflicts of interest

There are no conflicts to declare.

Notes and references

1 F. Wang, M. Yang, Y. Zhang, L. Yang, L. Fan, S. Lv, X. Liu, D. Han and J. Yang, *Adv. Sci.*, 2018, **6**, 1801170.
2 D. Baran, R. S. Ashraf, D. A. Hanifi, M. Abdelsamie, N. Gasparini, J. A. Rohr, S. Holliday, A. Wadsworth, S. Lockett, M. Neophytou, C. J. Emmott, J. Nelson, C. J. Brabec, A. Amassian, A. Salleo, T. Kirchartz, J. R. Durrant and I. McCulloch, *Nat. Mater.*, 2017, **16**, 363–369.
3 A. Tang, C. Zhan, J. Yao and E. Zhou, *Adv. Mater.*, 2017, **29**, 1600013.
4 D. Kiermasch, L. Gil-Escrig, A. Baumann, H. J. Bolink, V. Dyakonov and K. Tvingstedt, *J. Mater. Chem. A*, 2019, **7**, 14712–14722.
5 Y. Wang, J. Liu, Y. Ozaki, Z. Xu and B. Zhao, *Angew. Chem., Int. Ed.*, 2019, **58**, 8172–8176.
6 X. Su, H. Ma, H. Wang, X. Li, X. X. Han and B. Zhao, *Chem. Commun.*, 2018, **54**, 2134–2137.
7 Z. Yu, W. Yu, J. Xing, R. A. Ganeev, W. Xin, J. Cheng and C. Guo, *ACS Photonics*, 2018, **5**, 1619–1627.
8 X. Wang, P. Li, X. X. Han, Y. Kitahama, B. Zhao and Y. Ozaki, *Nanoscale*, 2017, **9**, 15303–15313.
9 J. F. Li, Y. J. Zhang, S. Y. Ding, R. Panneerselvam and Z. Q. Tian, *Chem. Rev.*, 2017, **117**, 5002–5069.
10 X. X. Han, W. Ji, B. Zhao and Y. Ozaki, *Nanoscale*, 2017, **9**, 4847–4861.
11 M. Yilmaz, E. Babur, M. Ozdemir, R. L. Gieseking, Y. Dede, U. Tamer, G. C. Schatz, A. Facchetti, H. Usta and G. Demirel, *Nat. Mater.*, 2017, **16**, 918–924.
12 J. R. Lombardi, *Nat. Mater.*, 2017, **16**, 878–880.
13 S. D. Kang and G. J. Snyder, *Nat. Mater.*, 2017, **16**, 252–257.
14 M. Hilal and J. I. Han, *Sol. Energy*, 2018, **174**, 743–756.
15 Y. Wang, C. Zhu, R. Pfattner, H. Yan, L. Jin, S. Chen, F. Molina-Lopez, F. Lissel, J. Liu, N. I. Rabiah, Z. Chen, J. W. Chung, C. Linder, M. F. Toney, B. Murmann and Z. Bao, *Sci. Adv.*, 2017, **3**, 2375–2548.
16 J. Casanovas, D. Zanuy and C. Aleman, *Phys. Chem. Chem. Phys.*, 2017, **19**, 9889.
17 J. A. L. Sánchez, R. P. Capilla and A. M. Díez-Pascual, *Polymers*, 2018, **10**, 1169.
18 W. P. Su, J. R. Schrieffer and A. J. Heeger, *Phys. Rev. Lett.*, 1979, **42**, 1698–1701.
19 W. P. Su, J. R. Schrieffer and A. J. Heeger, *Phys. Rev. B: Condens. Matter Mater. Phys.*, 1980, **22**, 2099–2111.
20 J. F. Yu, C. Q. Wu, X. Sun and K. Nasu, *Phys. Rev. B: Condens. Matter Mater. Phys.*, 2004, **70**, 064303.
21 A. A. Johansson and S. Stafström, *Phys. Rev. B: Condens. Matter Mater. Phys.*, 2004, **69**, 235205.
22 Z. Dai, G. Wang, X. Xiao, W. Wu, W. Li, J. Ying, J. Zheng, F. Mei, L. Fu, J. Wang and C. Jiang, *J. Phys. Chem. C*, 2014, **118**, 22711–22718.
23 S. D. Roy, P. Sett, M. Ghosh and J. Chowdhury, *J. Raman Spectrosc.*, 2017, **48**, 38–45.
24 M. Hilal and J. I. Han, *Appl. Nanosci.*, 2018, **8**, 1325–1341.
25 M. Yilmaz, M. Ozdemir, H. Erdogan, U. Tamer, U. Sen, A. Facchetti, H. Usta and G. Demirel, *Adv. Funct. Mater.*, 2015, **25**, 5669–5676.
26 J. R. Lombardi and R. L. Birke, *J. Phys. Chem. C*, 2014, **118**, 11120–11130.
27 O. Bubnova, Z. U. Khan, H. Wang, S. Braun, D. R. Evans, M. Fabretto, P. Hojati-Talemi, D. Dagnelund, J. B. Arlin, Y. H. Geerts, S. Desbief, D. W. Breiby, J. W. Andreasen, R. Lazzaroni, W. M. Chen, I. Zozoulenko, M. Fahlman, P. J. Murphy, M. Berggren and X. Crispin, *Nat. Mater.*, 2014, **13**, 190–194.
28 J. Rivnay, S. Inal, B. A. Collins, M. Sessolo, E. Stavrinidou, X. Strakosas, C. Tassone, D. M. Delongchamp and G. G. Malliaras, *Nat. Commun.*, 2016, **7**, 11287–11302.
29 X. Wang, W. Shi, S. Wang, H. Zhao, J. Lin, Z. Yang, M. Chen and L. Guo, *J. Am. Chem. Soc.*, 2019, **141**, 5856–5862.
30 X.-Y. Zhang, D. Han, Z. Pang, Y. Sun, Y. Wang, Y. Zhang, J. Yang and L. Chen, *J. Phys. Chem. C*, 2018, **122**, 5599–5605.
31 S. Y. Ding, E. M. You and Z. Q. Tian, *Chem. Soc. Rev.*, 2017, **46**, 4042–4076.
32 R. L. Gieseking, M. A. Ratner and G. C. Schatz, *Faraday Discuss.*, 2017, **205**, 149–171.
33 X.-Y. Zhang, D. Han, N. Ma, R. Gao, A. Zhu, S. Guo, Y. Zhang, Y. Wang, J. Yang and L. Chen, *J. Phys. Chem. Lett.*, 2018, **9**, 6047–6051.
34 C. Boerigter, U. Aslam and S. Linic, *ACS Nano*, 2016, **10**, 6108–6115.
35 X.-C. Ma, Y. Dai, L. Yu and B.-B. Huang, *Light: Sci. Appl.*, 2016, **5**, e16017.
36 Z. Mao, W. Song, X. Xue, W. Ji, Z. Li, L. Chen, H. Mao, H. Lv, X. Wang, J. R. Lombardi and B. Zhao, *J. Phys. Chem. C*, 2012, **116**, 14701–14710.
37 J. R. Lombardi, R. L. Birke, L. A. Sanchez, I. Bernard and S. C. Sun, *Chem. Phys. Lett.*, 1984, **104**, 240–247.
38 I. Hisao, S. Kiyoshi, I. Eisuke and S. Kazuhiko, *Adv. Mater.*, 1999, **11**, 605–625.
39 V. G. Rao, U. Aslam and S. Linic, *J. Am. Chem. Soc.*, 2019, **141**, 643–647.
40 G. Su, S. Yang, S. Li, C. J. Butch, S. N. Filimonov, J. C. Ren and W. Liu, *J. Am. Chem. Soc.*, 2019, **141**, 1628–1635.
41 H. Shi, C. Liu, Q. Jiang and J. Xu, *Adv. Electron. Mater.*, 2015, **1**, 1500017.
42 Y. Xia and J. Ouyang, *ACS Appl. Mater. Interfaces*, 2010, **2**, 474–483.

